Optical and Scintillation Properties of YAlO$_3$ Doped with Rare-earth Ions Emitting Near-infrared Photons

Masaki Akatsuka,[*] Daisuke Nakauchi, Takumi Kato,
Noriaki Kawaguchi, and Takayuki Yanagida

Division of Materials Science, Nara Institute of Science and Technology, 8916-5 Takayama,
Ikoma, Nara 630-0192, Japan

Scintillators emitting near-infrared (NIR) photons have unique characteristics and have been attracting attention recently. For example, scintillators emitting NIR photons are expected to be effective tools for radiation dose monitoring in high-dose environments. In this study, YAlO$_3$ samples doped with various rare-earth ions (Er^{3+}, Ho^{3+}, Pr^{3+}, and Tm^{3+}) were synthesized by the floating zone method and their scintillation properties from the UV to NIR range were evaluated. Regarding their scintillation detection property, the Er^{3+}-doped sample indicated an approximately linear proportional relationship from 1 mGy to 10 Gy.

1. Introduction

Inorganic scintillators are fluorescent materials that rapidly convert ionizing radiation to several thousands of low-energy photons.[1] They have been used widely in various fields such as medical imaging,[2] security,[3] environmental monitoring,[4] and high-energy physics.[5] Most of the recently developed inorganic scintillators consist of a host material and an emission center. The host material affects the absorption of ionizing radiation, and the emission center emits scintillation photons. Generally, rare-earth (RE) ions with a bright emission due to 5d–4f transitions are selected as an emission center in inorganic scintillators.[6–10] On the other hand, RE ions with an emission due to 4f–4f transitions have also been studied[11,12] for phosphor applications. For example, Nd^{3+} and Yb^{3+} are commonly used in a near-infrared (NIR) laser material.[13–15] In recent years, scintillators emitting NIR photons have attracted considerable attention because of their unique characteristics. NIR photons have a high penetration power into the human body without fatal damage.[16,17] Since the optical window is from 700 to 1200 nm for the human body, NIR-emitting scintillators can be used for radiation-based bioimaging applications.[18] Furthermore, scintillators emitting NIR photons are expected to be effective tools for radiation dose monitoring in high-dose environments. In general, high-dose environments such as a nuclear reactor generate Cherenkov radiation, which has very high intensity and is observed in the UV–blue range. If scintillator materials emitting UV–blue light

are used in high-dose environments, the Cherenkov radiation overlaps with scintillation signals and causes incorrect radiation measurements. In such cases, NIR-emitting scintillators work advantageously because NIR signals are easily distinguished from the Cherenkov noise.[19]

Recently, we have studied scintillators emitting NIR photons (600–1650 nm) such as fluorides,[19] sesquioxides,[20] oxide garnets,[21] and oxide perovskites.[22,23] For these scintillators, Nd^{3+} and Yb^{3+} are used as NIR emission centers. On the other hand, some RE ions, other than Nd^{3+} and Yb^{3+}, show luminescence in the NIR range.[24,25] Above all, Er^{3+}, Ho^{3+}, Pr^{3+}, and Tm^{3+} show luminescence in the 700–1200 nm range, which corresponds to the optical window of the human body. In this work, $YAlO_3$ samples doped with 1% each of Er^{3+}, Ho^{3+}, Pr^{3+}, and Tm^{3+} were synthesized and evaluated for their photoluminescence (PL) and scintillation properties. To the best of our knowledge, there have been no studies on NIR scintillation properties of $YAlO_3$ samples doped with 1% each of Er^{3+}, Ho^{3+}, Pr^{3+}, and Tm^{3+}.

2.   Materials and Methods

$YAlO_3$ samples doped with 1% each of Er^{3+}, Ho^{3+}, Pr^{3+}, and Tm^{3+} were synthesized by the optical floating zone (FZ) method.[26,27] The concentrations of REs added were with respect to that of Y. The raw material powders used were Y_2O_3, Al_2O_3, Er_2O_3, Ho_2O_3, Pr_2O_3, and Tm_2O_3. They were mixed to the compositions shown above. After mixing, the powders were formed into rods by applying hydrostatic pressure. After the shaping process, the rods of all the compositions were sintered at 1200 °C for 8 h in air to obtain ceramic rods. The FZ furnace used in this study was FZD0192, Canon Machinery. During crystal growth, the rotation rate was 20 rpm, and the pull-down rate was modulated within the range of 2.5–5.0 mm/h in order to stabilize the molten zone.

The PL excitation/emission contour spectrum (PL map) and PL quantum yield (QY) were measured using a Quantaurus-QY (C11347, Hamamatsu). The excitation and emission wavelengths ranges for the PL map were 250-800 and 300–950 nm, respectively. The measurement interval for excitation wavelengths was 10 nm. The absolute QY was calculated as $QY = N_{emit}/N_{absorb}$, where N_{emit} and N_{absorb} are the numbers of emitted and absorbed photons, respectively. PL decay time profiles were evaluated using a Quantaurus-τ (C11367, Hamamatsu), and the excitation and monitoring wavelengths were selected on the basis of the obtained PL map.

As a scintillation property, X-ray-induced scintillation spectra were measured by applying our original setup.[9] The excitation source was an X-ray generator (XRB80N100/CB, Spellman) equipped with a conventional X-ray tube having a W anode target and a Be window, supplied with a bias voltage of 60 kV and a tube current of 1.0 mA. The emission spectra were measured using the following two different spectrometers to cover a wide spectral range from UV to NIR: Andor DU-420-BU2 for 180–700 nm and Andor DU492A for 650–1650 nm. These CCD-based detectors were coupled with a monochromator, Shamrock 163. Each spectrometer was placed off the irradiation axis, and the scintillation light was guided into the spectrometer through a 2 m optical fiber to prevent the direct exposure of the CCD to X-rays. In addition, as a detector property, we measured the relationship between the integrated scintillation intensity

and the X-ray exposure doses in the NIR wavelength range from 1 mGy to 10 Gy by controlling the tube current and irradiation time. Moreover, scintillation decay time profiles were measured using an afterglow characterization system equipped with a pulse X-ray tube.[28] The system enabled us to perform measurements by time-correlated single-photon counting (TCSPC). The PMT used in this measurement covered the spectral range from 400 to 900 nm. The voltage applied to the pulse X-ray source was 30 kV, and the system offered a timing resolution of ~1 ns in the shortest time range. For both the PL and scintillation decay time profiles, the decay time constant was deduced by least squares fitting with an exponential decay function.

3.   Results and Discussion

The typical dimensions of as-synthesized rods were 4 mm in diameter and 15–20 mm in length. For characterization, the grown crystal rods were cut into small pieces. Figure 1 shows a photograph of the synthesized $YAlO_3$ samples doped with 1% REs. All samples look translucent with many small cracks. Moreover, the 1% Ho^{3+}-doped sample looks white, the 1% Pr^{3+}-doped sample looks green, and the 1% Er^{3+}- and Tm^{3+}-doped samples look colorless.

Figure 2 shows powder X-ray diffraction (XRD) patterns of $YAlO_3$ samples doped with 1% REs. The XRD pattern of $YAlO_3$ (JCPDS #87-1290) is also shown for comparison. All the samples seem to have a perovskite single phase, which belongs to the $Pm\bar{3}m$ space group of a cubic crystal system.

The PL maps of all the samples are shown in Fig. 3. The strong emissions of the 1% Er^{3+}-doped sample were observed at around 550 nm ($^4S_{3/2} \rightarrow {}^4I_{15/2}$) and 850 nm ($^4S_{3/2} \rightarrow {}^4I_{13/2}$).[29,30] The 1% Ho^{3+}-doped sample showed strong emissions of around 550 nm ($^5F_4, {}^5S_2 \rightarrow {}^5I_8$) and 750 nm ($^5S_2 \rightarrow {}^5I_7$).[29,31] The 1% Pr^{3+}-doped sample showed the strong emissions of around 500 nm ($^3P_0 \rightarrow {}^3H_4$), 610 nm ($^1D_2 \rightarrow {}^3H_4$), and 750 nm ($^3P_0 \rightarrow {}^3F_4$).[32,33] The 1% Tm^{3+}-doped sample indicated strong emissions of around 450 nm ($^1D_2 \rightarrow {}^3F_4$) and 800 nm ($^3H_4 \rightarrow {}^3H_6$).[34,35]
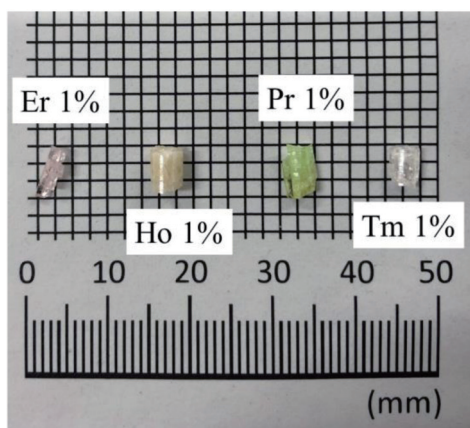

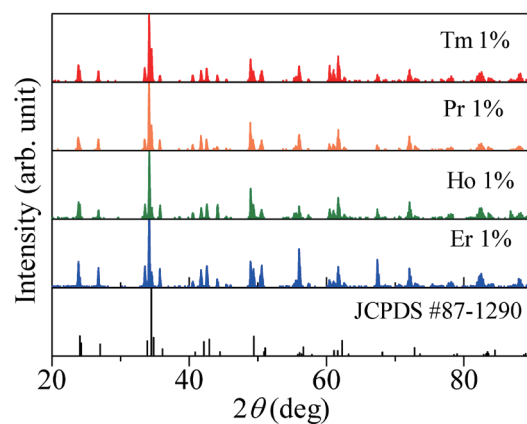Fig. 1.   (Color online) Photograph of $YAlO_3$ samples doped with 1% REs.

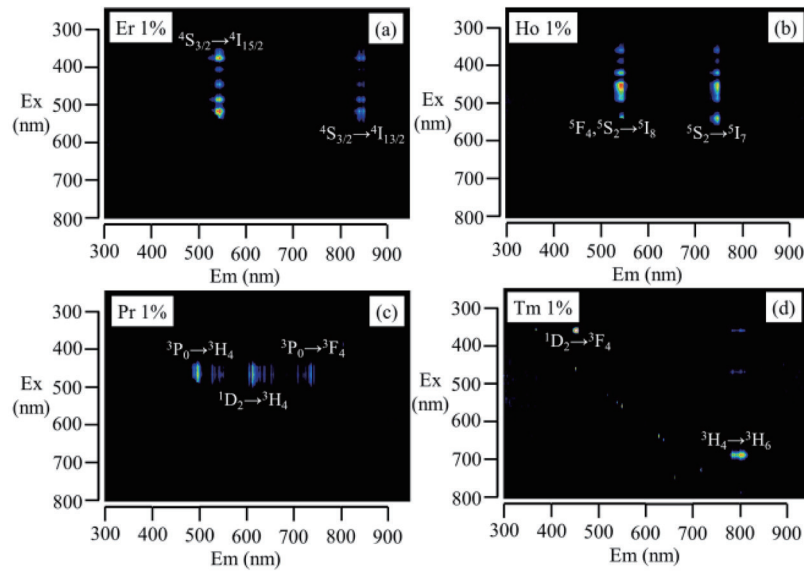Fig. 2.   (Color online) Powder XRD patterns of synthesized $YAlO_3$ samples doped with 1% REs.

Fig. 3. (Color online) PL maps of synthesized YAlO$_3$ samples doped with 1.0% (a) Er^{3+}, (b) Ho^{3+}, (c) Pr^{3+}, and (d) Tm^{3+}. The horizontal and vertical axes show emission and excitation wavelengths, respectively.

Table 1
QY values of YAlO$_3$ samples doped with 1% RE in the ranges of (a) 200–700 and (b) 700–950 nm.

Sample	QY (Em. 200–700 nm)	QY (Em. 700–950 nm)
YAlO$_3$:Er^{3+}	13.8 %	6.6%
YAlO$_3$:Ho^{3+}	6.3%	3.8%
YAlO$_3$:Pr^{3+}	20.3%	8.4%
YAlO$_3$:Tm^{3+}	13.9%	22.1%

Here, QY values of all the samples were calculated by the integration of signal intensity in the range from 200 to 700 nm and 700 to 950 nm in order to divide the UV–VIS emission from the NIR emission, and the obtained results are summarized in Table 1. Among all the samples, the 1% Pr^{3+}-doped sample showed the highest QY in the UV–VIS range, and the 1% Tm^{3+}-doped sample showed the highest QY in the NIR range.

Figure 4 shows the PL decay curves of all the samples. Here, the monitoring wavelengths were around 840 nm (Er^{3+}), 760 nm (Ho^{3+}), 720 nm (Pr^{3+}), and 800 nm (Tm^{3+}), and the excitation wavelengths were 460–510 nm. The obtained curves of all the samples was approximated by a single exponential decay function. For all the samples, the PL decay time constants of 4f–4f transitions of Er^{3+}, Ho^{3+}, Pr^{3+}, and Tm^{3+} were 108, 33, 15, and 432 μs, respectively. These decay times agreed with those previously reported.[32,36–38]

Figure 5 shows X-ray-induced scintillation spectra measured in the (a) UV–VIS and (b) NIR ranges. All the samples showed emission lines due to the 4f–4f transitions of RE ions. The observed dominant emissions by the RE ions were as follows: emissions by Er^{3+} were identified as the electronic transitions of ^{2}H$_{9/2}$→^{4}I$_{15/2}$ (400 nm), ^{4}F$_{5/2}$→^{4}I$_{15/2}$ (470 nm), ^{4}S$_{3/2}$→^{4}I$_{15/2}$ (550 nm), ^{4}S$_{3/2}$→^{4}I$_{13/2}$ (830 nm), ^{4}I$_{11/2}$→^{4}I$_{15/2}$ (1000 nm), and ^{4}I$_{13/2}$→^{4}I$_{15/2}$ (1550 nm);[39,40]
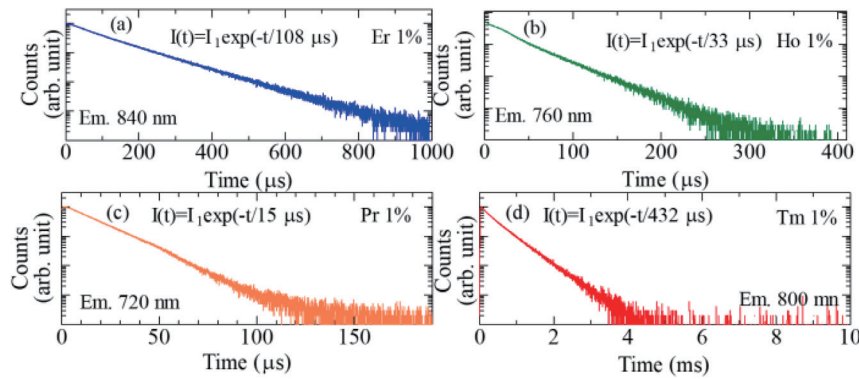
Fig. 4.   (Color online) PL decay curves of synthesized YAlO$_3$ samples doped with 1% (a) Er^{3+}, (b) Ho^{3+}, (c) Pr^{3+}, and (d) Tm^{3+}. The excitation wavelengths were 460–510 nm.
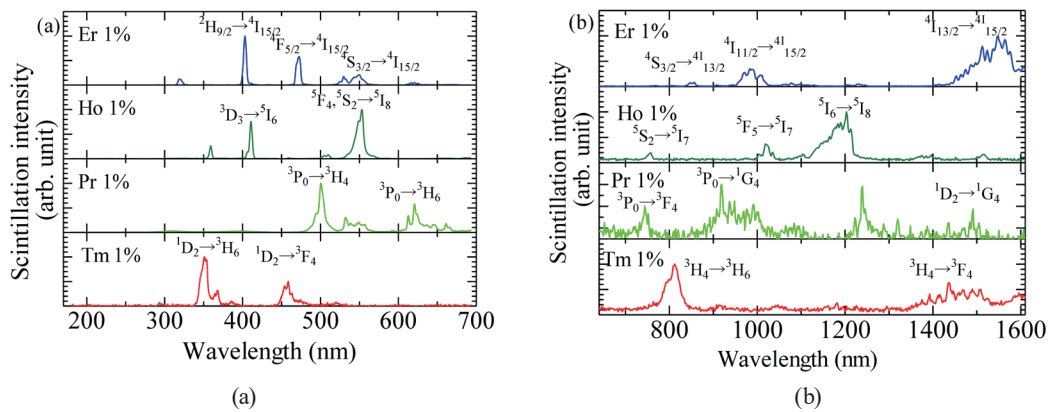

Fig. 5.   (Color online) X-ray-induced scintillation spectra of YAlO$_3$ samples doped with REs in the (a) UV-VIS and (b) NIR ranges.

emissions by Ho^{3+} were identified as the electronic transitions of $^3D_3 \rightarrow {}^5I_6$ (410 nm), $^5F_4, {}^5S_2 \rightarrow {}^5I_8$ (550 nm), $^5S_2 \rightarrow {}^5I_7$ (780 nm), $^5F_5 \rightarrow {}^5I_7$ (1010 nm), and $^5I_6 \rightarrow {}^5I_8$ (1200 nm);[24,31] emissions by Pr^{3+} were identified as the electronic transitions of $^3P_0 \rightarrow {}^3H_4$ (500 nm), $^3P_0 \rightarrow {}^3H_6$ (610 nm), $^3P_0 \rightarrow {}^3F_4$ (780 nm), $^3P_0 \rightarrow {}^1G_4$ (960 nm), and $^1D_2 \rightarrow {}^1G_4$ (1500 nm);[24,32,41] emissions by Tm^{3+} were identified as the electronic transitions of $^1D_2 \rightarrow {}^3H_6$ (350 nm), $^1D_2 \rightarrow {}^3F_4$ (460 nm), $^3H_4 \rightarrow {}^3H_6$ (800 nm), and $^3H_4 \rightarrow {}^3F_4$ (1400 nm).[34,42] Furthermore, the 1% Pr^{3+}-doped sample showed other emissions from 1000 to 1300 nm. These emissions could not be identified as the Pr^{3+} 4f–4f transitions. Here, we considered that these emissions were diffraction light from 500 to 650 nm.

As a detector property, the relationship between the integration value from 640 to 1620 nm and the X-ray exposure dose was evaluated as shown in Fig. 6. The obtained dynamic ranges of Er^{3+}-, Tm^{3+}-, and Ho^{3+}-doped samples were 1–10000, 10–10000, and 10–10000 mGy, respectively.

Figure 7 shows X-ray-induced scintillation decay time profiles. The decay curves of the 1% Ho^{3+}-doped sample were approximated by a single exponential decay function, and the decay
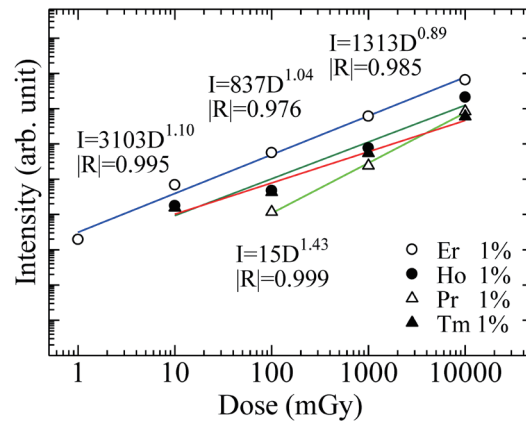
Fig. 6.   (Color online) Relationship between integrated value from 640 to 1620 nm and X-ray exposure dose from 1 mGy to 10 Gy in NIR wavelength range of YAlO$_3$ samples doped with 1% REs.
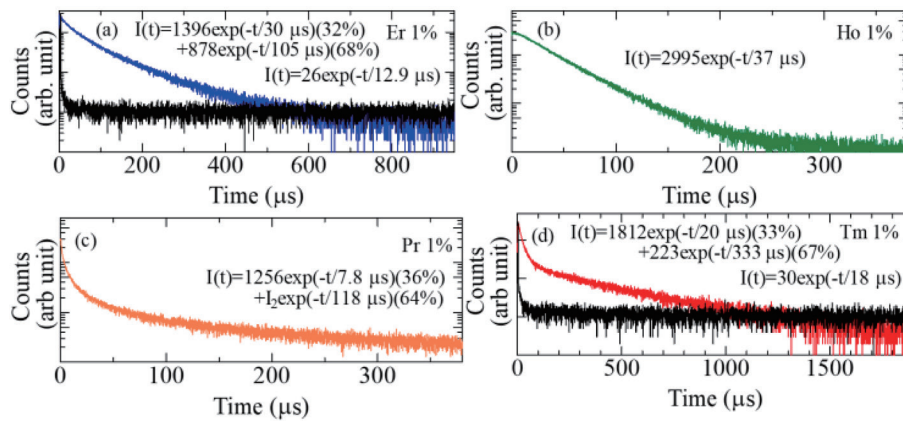

Fig. 7.   (Color online) X-ray-induced scintillation decay curves of synthesized YAlO$_3$ samples doped with 1% (a) Er^{3+}, (b) Ho^{3+}, (c) Pr^{3+}, and (d) Tm^{3+}.

time was found to be similar to the PL decay time. Thus, the origin of the observed emission was identified as the 4f–4f transition of Ho^{3+}. The other decay curves of all the samples were approximated by the sum of two exponential decay functions. In the 1% Er^{3+}- and 1% Tm^{3+}-doped samples, the longer decay times were similar to the PL decay time. Therefore, the slower-decay components were due to the 4f–4f electronic transitions of RE ions (Er^{3+} and Tm^{3+}). From the result of the instrumental response function, the faster-decay component of the 1% Er^{3+}-doped sample was considered to be due to lattice defects, and that of the 1% Tm^{3+}-doped sample to be due to the instrumental response. On the other hand, in the 1% Pr^{3+}-doped sample, the faster-decay component was similar to the PL decay time component. Thus, the shorter decay time of the 1% Pr^{3+}-doped sample could be due to the 4f–4f transition of Pr^{3+}. The longer decay time is considered to be caused by the emission due to lattice defects.

4. Conclusions

We evaluated the PL and scintillation properties of YAlO$_3$ samples doped with 1% REs such as Pr, Ho, Er, and Tm. In the PL map, all the samples showed strong emissions due to the 4f–4f transitions of RE ions, and the 1% Tm^{3+}-doped sample showed the highest QY in the NIR range. The PL decay curves of all the samples could be approximated by a single exponential decay function, and the scintillation decay curves could be approximated by one or two exponential decay functions. Regarding their scintillation detection property, the 1% Er^{3+}-doped sample indicated a proportional relationship from 1 to 10000 mGy.

Acknowledgments

References

1   T. Yanagida: Proc. Japan Academy, Ser. B, Physical and Biological Sciences **94** (2018) 75.
2   Y. Hirata, K. Watanabe, S. Yoshihashi, A. Uritani, Y. Koba, N. Matsufuji, T. Yanagida, T. Toshito, and K. Fukuda: Sens. Mater. **29** (2017) 1455.
3   J. Glodo, Y. Wang, R. Shawgo, C. Brecher, R. H. Hawrami, J. Tower, and K. S. Shah: Physics Procedia **90** (2017) 285.
4   J. N. Kim, M. H. Ryu, Y. S. Yang, and J. Chang: Sens. Mater. **27** (2015) 585.
5   T. Itoh, T. Yanagida, M. Kokubun, M. Sato, R. Miyawaki, K. Makishima, T. Takashima, T. Tanaka, K. Nakazawa, T. Takahashi, N. Shimura, and H. Ishibashi: Nucl. Instrum. Methods Phys. Res., Sect. A **579** (2007) 239.
6   N. Kawaguchi, H. Kimura, M. Akatsuka, G. Okada, N. Kawano, K. Fukuda, and T. Yanagida: Sens. Mater. **30** (2018) 1585.
7   H. Fukushima, D. Nakauchi, N. Kawaguchi, and T. Yanagida: Sens. Mater. **31** (2019) 1273.
8   D. Nakauchi, G. Okada, N. Kawano, N. Kawaguchi, and T. Yanagida: Appl. Phys. Express. **10** (2017) 072601.
9   T. Yanagida, K. Kamada, Y. Fujimoto, H. Yagi, and T. Yanagitani: Opt. Mater. **35** (2013) 2480.
10 F. Nakamura, T. Kato, G. Okada, N. Kawaguchi, K. Fukuda, and T. Yanagida: Ceram. Int. **43** (2017) 604.
11 Y. Shi, Q. W. Chen, and J. L. Shi: Opt. Mater. **31** (2009) 729.
12 T. Yanagida: Opt. Mater. **35** (2013) 1987.
13 J. J. Zayhowski and C. Dill: Opt. Lett. **19** (1994) 1427.
14 J. E. Geusic, H. M. Marcos, and L. G. Van Uitert: Appl. Phys. Lett. **4** (1964) 182.
15 K. Soga, T. Tsuji, F. Tashiro, J. Chiba, M. Oishi, K. Yoshimoto, Y. Nagasaki, K. Kitano, and S. Hamaguchi: J. Phys. Conf. Ser. **106** (2008) 012023.
16 J. L. Boulnois: Lasers Med. Sci. **1** (1986) 47.
17 L. Sudheendra, G. K. Das, C. Li, D. Stark, J. Cena, S. Cherry, and I. M. Kennedy: Chem. Mater. **26** (2014) 1881.
18 K. Toh, T. Nakamura, H. Yamagishi, K. Sakasai, K. Soyama, and T. Shikama: Nucl. Instrum. Methods Phys. Res., Sect. A **700** (2013) 130.
19 T. Yanagida, Y. Fujimoto, S. Ishizu, and K. Fukuda: Opt. Mater. **41** (2015) 36.
20 T. Yanagida, Y. Fujimoto, H. Yagi, and T. Yanagitani: Opt. Mater. **36** (2014) 1044.
21 T. Oya, G. Okada, and T. Yanagida: J. Ceram. Soc. Japan. **124** (2016) 536.

22 M. Akatsuka, Y. Usui, D. Nakauchi, G. Okada, N. Kawaguchi, and T. Yanagida: Sens. Mater. **30** (2018) 1525.
23 M. Akatsuka, Y. Usui, D. Nakauchi, T. Kato, N. Kawano, G. Okada, N. Kawaguchi, and T. Yanagida: Opt. Mater. **79** (2018) 428.
24 L. Sun, Y. Qiu, T. Liu, J. Z. Zhang, S. Dang, J. Feng, Z. Wang, H. Zhang, and L. Shi: ACS Appl. Mater. Interfaces **5** (2013) 9585.
25 G. Okada, N. Kawaguchi, and T. Yanagida: Sens. Mater. **29** (2017) 1407.
26 T. Akashi, K. Matumi, T. Okada, and T. Mizutani: IEEE Trans. Magn. **5** (1969) 285.
27 D. Nakauchi, G. Okada, N. Kawaguchi, and T. Yanagida: Jpn. J. Appl. Phys. **57** (2018) 100307.
28 T. Yanagida, Y. Fujimoto, T. Ito, K. Uchiyama, and K. Mori: Appl. Phys. Express **7** (2014) 062401.
29 N. Kumamoto, D. Nakauchi, T. Kato, G. Okada, N. Kawaguchi, and T. Yanagida: Sens. Mater. **29** (2017) 1417.
30 S. F. León-Luis, U. R. Rodríguez-Mendoza, P. Haro-González, I. R. Martín, and V. Lavín: Sens. Actuators, B **174** (2012) 176.
31 L. Feng, J. Wang, Q. Tang, L. Liang, H. Liang, and Q. Su: J. Lumin. **124** (2007) 187.
32 G. Özen, O. Forte, B. Di Bartolo, and J. M. Collins: J. Lumin. **125** (2007) 223.
33 L. Vijayalakshmi, V. Naresh, B. H. Rudramadevi, and S. Buddhudu: Int. J. Eng. Sci. **4** (2014) 19.
34 P. Camy, J. L. Doualan, S. Renard, A. Braud, V. Ménard, and R. Moncorgé: Opt. Commun. **236** (2004) 395.
35 N. Kawano, D. Nakauchi, K. Fukuda, G. Okada, N. Kawaguchi, and T. Yanagida: Jpn. J. Appl. Phys. **57** (2018) 102401.
36 S. Coffa, G. Franzò, F. Priolo, A. Polman, and R. Serna: Phys. Rev. B **49** (1994) 16313.
37 F. Qin, Y. Zheng, Y. Yu, Z. Cheng, P. S. Tayebi, W. Cao, and Z. Zhang: J. Alloys Compd. **509** (2011) 1115.
38 P. Y. Poma, K. U. Kumar, M. V. D. Vermelho, K. Serivalsatit, S. A. Roberts, C. J. Kucera, J. Ballato, L. G. Jacobsohn, and C. Jacinto: J. Lumin. **161** (2015) 306.
39 A. C. S. De Mello, A. B. Andrade, G. H. G. Nakamura, S. L. Baldochi, and M. E. G. Valerio: J. Lumin. **138** (2013) 19.
40 C. Quan, D. Sun, J. Luo, H. Zhang, Z. Fang, X. Zhao, L. Hu, M. Cheng, Q. Zhang, and S. Yin: Opt. Mater. **84** (2018) 59.
41 X. Zhou, G. Wang, K. Zhou, and Q. Li: Opt. Mater. **35** (2013) 600.
42 N. Kawano, N. Kawaguchi, G. Okada, Y. Fujimoto, and T. Yanagida: Sens. Mater. **30** (2018) 1539.